Processing and evaluation of dissimilar Al-SS friction welding of pipe configuration: nondestructive inspection, properties, and microstructure

Hardik D. Vyas[1], Kush P. Mehta[1, 2 *], Vishvesh Badheka[1], Bharat Doshi[3]

[1]Department of Mechanical Engineering, School of Technology, Pandit Deendayal Petroleum University, Raisan, Gandhinagar, Gujarat, India.

[2]Advanced Manufacturing and Materials group, Department of Mechanical Engineering, School of Engineering, Aalto University, Espoo, Finland

[3]Institute for Plasma Research, Gandhinagar, Gujarat, India.

[*]Corresponding author: kush_2312@yahoo.com, kush.mehta@aalto.fi

Abstract

In the present investigation, dissimilar Al-SS friction welding of pipe joint configuration with an outer diameter of 88.90 mm and a wall thickness of 5.4 mm was performed. Four different experimental conditions were varied based on visual inspection after each weld. The welded pipe joints were evaluated by vacuum leak detection, thermal shock test, pneumatic pressure test, tensile test, optical and scanning electron microscopies, energy dispersive X-ray spectroscopes, X-ray diffractions, X-ray elemental mapping, and line hardness measurements. The results revealed that friction welded Al-SS bimetallic pipes can sustain ultra-high vacuum pressure and cryogenic working environments without leak detection. Al-SS friction welded pipe resulted in high tensile strength with 72% of joint efficiency as compared to AA6063-T6 base material. Microstructure influences were observed largely in the AA6063-T6 side close to the Al-SS interface. The intermetallic compound of Fe_3Al phase was identified with a reaction layer between Al-SS joints with varying thickness of 1.1 μm to 2.0 μm.

Keywords: Al-SS, dissimilar welding, friction welding, pipe joints, microstructure, properties

1. Introduction

Developments in dissimilar welded joints with an interesting combination of multi-materials and complex joint configurations are continuously growing for different industrial applications with exciting knowledge on joint properties under different processing actions [1]; though it has proved to be a revolutionary technology, there are many combination of dissimilar materials for example Cu-SS [2], dissimilar aluminum alloys [3], Al-Mg [4], Al-AZ31B [5], Mg-Ti [6], Al-Cu [7-9] presents practical challenges. Also, the combination of the manufacturing processes is an advantage for developing dissimilar metal joints [7]. The solid-state joining is helpful to build high quality joint for dissimilar materials due to capabilities to handle metallurgical complexities [8-9]. Dissimilar materials combination of aluminum (Al) and stainless steel (SS) is one of those interesting bimetal joints applied in various industries with a variety of applications such as cryogenic heat exchangers' transition joint, automotive structural joints, vacuum applications, rocket's propulsion systems and many more [10]. Cost and weight reduction benefits can be greatly obtained with density differences of Al and SS along with an advantage of hybrid properties of components [11-12]. Despite interesting applications and great benefits, the welding of Al-SS combination is a challenging task owing to intermetallic compounds (IMCs) formation and metallurgical complexity in materials mixing within the welding region caused by dissimilarities in the physical, chemical and mechanical behavior of Al and SS materials [13]. The formation of IMCs and other metallurgical discontinuities are prominent in the case of fusion based welding due to solubility issues and hence solid state-based welding processes are recommended for dissimilar joints [14]. Friction based welding processes are operated with a solid-state processing concept, using frictional heat and mechanical pressure as governing factors to obtain metallurgical strong welds [15]. Therefore, friction-based welding is successfully applied to Al-steel combination [16].

Paventhan et al. [17] performed friction welding on AA6082-T6 and stainless steel (SS) of AISI 304 for a solid round bar of a 12 mm diameter. They observed maximum 213 MPa of UTS in their optimized parameters. Similarly, the rotary friction welding process adopted by Alves et al. [18], performed for a AA1050 and AISI 304, using a solid round bar of 14.8 mm diameter, wherein they obtained 80.08 MPa ultimate tensile strength of joint. Fukumoto et al. [19] studied the friction welding process for a diameter of 16 mm round bar workpiece of pure AA1050 and SS304. They observed that in shorter friction time, the hardness of Al alloy increased near to joint region. Lee et al.[20] investigated friction welding parameters for AA5052 alloy to A36 steel joints for a 20 mm diameter of a solid bar. They observed extended

grain structure with dynamic recrystallization towards the Al material and no deformation in the A36 steel material. They found that the process parameters of friction time and upset pressure are critical for friction welding. Yokoyama et al. [21] investigated friction welding of a 12 mm diameter of a solid round bar for AA6061-SS304 dissimilar joints. They varied upset pressure and friction time keeping other parameters constant and obtained maximum tensile strength of 299.2 MPa. Kimura et al. [22] investigated AA6063-SS304 combination with a 12 mm diameter of cylindrical rod using friction welding. They claimed 100% joint efficiency with 90 % of ductility. Fukumoto et al. [23] studied three different dissimilar joints of AA1050/SS304, AA5052/SS304, and AA6061/SS304 with friction welding for a solid round bar. They mentioned that the thin reaction layer between Al-SS materials influences tensile strength of joint. Yilmaz et al. [24] characterized the joint interface of Al-SS friction welding for 9.5 mm cylindrical rod. They found that the formation of IMCs can be greatly influenced by friction time, wherein the thickness of IMCs plays a critical role. Meshram et al. [25] performed experiments on dissimilar AISI 4340 to AA6061-T6 friction welding for 15 mm solid cylindrical bar, with an interlayer of sliver pre-applied by electroplating on AISI 4340 side. The tensile strength and elongation to fracture were improved with interlayer coating as compared to the one without interlayer application. Wang et al. [26] investigated Al-SS welds for a 15 mm diameter of round bar using friction welding. They obtained 88 % joint efficiency and 80° bend angle.

It can be noted that majority of investigations were performed with cylindrical rod configuration with fewer challenges on meeting surfaces for friction and holding of workpieces in fixtures. Limited articles are available on pipe joint configurations addressing thin meeting surfaces with large diameters. Kimura et al. [27] performed pipe configuration for Al-SS system using friction welding, mentioning as difficult configuration with a ratio of pipe thickness to the outside diameter below 0.1. However, they used a 14 mm diameter of pipe with inappropriate testing methods without removing flash from the welds. In another study of Al-SS pipe friction welding by Vyas et al. [10], the diameter of the pipe was around 60 mm, wherein the obtained joint efficiency was 60 %. The improvement in the joint efficiency and friction welding for higher diameter applications is still an active area of research. It is worth to perform Al-SS welding on higher diameter pipes with small thickness, keeping industrial applications of cryogenic bimetallic joints for heat exchangers applications and vacuum system pipes in view. Therefore, in the present study, dissimilar Al-SS friction welding was performed on 88.90 mm diameter with 5.4 mm thickness (i.e. ratio of pipe thickness to diameter is 0.060)

with four different conditions. Nondestructive inspection, microstructures and mechanical properties of Al-SS joints are investigated for this higher size pipe configuration welding.

2. Materials and Methods

Al alloy of heat-treated and artificially aged AA6063-T6 and SS 304L with its pipe diameter of 88.90 mm, and a wall thickness of 5.4 mm were used as workpiece materials in the present investigation. The chemical compositions and properties of the base materials are shown in Table 1 and Table 2 respectively.

Table 1. Chemical compositions of base materials

SS 304L	C	Mn	Si	Cr	Ni	P	S	Fe	
wt. %	0.028	1.14	0.36	18.36	8.2	0.026	0.002	Balance	
AA6063-T6	Mg	Si	Cu	Fe	Mn	Cr	Zn	Ti	Al
wt. %	0.50	0.39	0.036	0.12	0.019	0.024	0.002	0.012	98.80

Table 2. Mechanical and physical properties of base materials

Base material	Yield strength, MPa	Ultimate tensile strength, MPa	% Elongation	Melting point, °C	Coefficient of thermal expansion, K^{-1}	Thermal conductivity, W/m*k	Specific heat, J/kg*K
SS 304L	206	517	76.56	1454	17.3×10^{-6}	16.2	500
AA6063-T6	246.83	268.81	16.22	650	2.34×10^{-5}	218	900

Friction welding was performed on a fully automatic continuous drive friction welding machine of ETA make (model 150T). To protect deformation from spindle fixture, AA6063-T6 pipe was fixed on stationary fixture, whereas SS304L was fixed on a rotating side in the spindle fixture for all the experiments. The contact surfaces of both the workpieces were grinded and cleaned with the acetone before processing that helps to remove foreign materials and oxides from the surfaces. Different parametric combinations were performed to obtain welds keeping rotational speed and upset time constant as 350 rpm and 5 seconds respectively. These constant parameters were selected based on the previous study of Vyas et al. [10]. The variations in friction time, friction force, upset pressure, and burn off length are shown in Table

3, which were varied based on visual inspection of flash one by another. The visual inspection was carried out for flash formation and subsequent variation in parameters was performed.

After removing the flash from outer and inner surfaces from the pipe joints using turning and boring operations on lathe machine, these four different conditions were further analyzed with vacuum leak detection, thermal shock test, pneumatic pressure test, and tensile test. The best condition based on output from the aforementioned tests was characterized by microstructural analysis with optical and scanning electron microscopy (SEM), energy dispersive X-ray (EDX) spectroscopes, X-ray diffractions (XRD), X-ray elemental mapping and line hardness measurements. FE-SEM JEOL JSM 7600F model was used for SEM-EDX. XRD was performed using discover 8.0-Bruker.

Table 3. Processing parameters of friction welding

Experiment	Friction time (seconds)	Friction force (Tones)	Upset pressure (Tones)	Burn off length (mm)
1	3	2.2	4.4	4.067
2	5	4	3	5.03
3	15	8.2	16.4	25.1
4	18	10	12	22.55

The vacuum leak detection testing machine of mass spectrometer leak detector (MSLD) was used to perform the test, wherein samples of welded pipes were closed from both the ends using reducer and plate fixed using gas tungsten arc welding in order to mount it on machine. The vacuum leak detection experimental setup (Pfeiffer make of ASM 340 helium leak detector model) is shown in Figure 1. The helium was sprayed on the welded region, keeping sample on vacuum testing machine with background and initial readings of vacuum pressure. This testing was performed two times such as firstly with room temperature and secondly after the thermal shock test. For the thermal shock test, the welded samples were dipped in the liquid nitrogen fluid for 5 minutes keeping the temperature of 77 K. Next, the samples were pulled out from the liquid nitrogen container and kept aside in the atmospheric conditions until the temperature reached to a room temperature of 300 K. This process of thermal shock test was

reaffirmed three times. After the thermal shock test cycles, the samples were subjected to a vacuum testing. A pneumatic pressure test using helium gas was performed on all the samples under the pressure effect of 25 bar. Nondestructive testing of vacuum, thermal shock, and pressure tests were performed to check the sustainability of cryogenic and vacuum environment working conditions of AA6063T6-SS304L dissimilar joints.

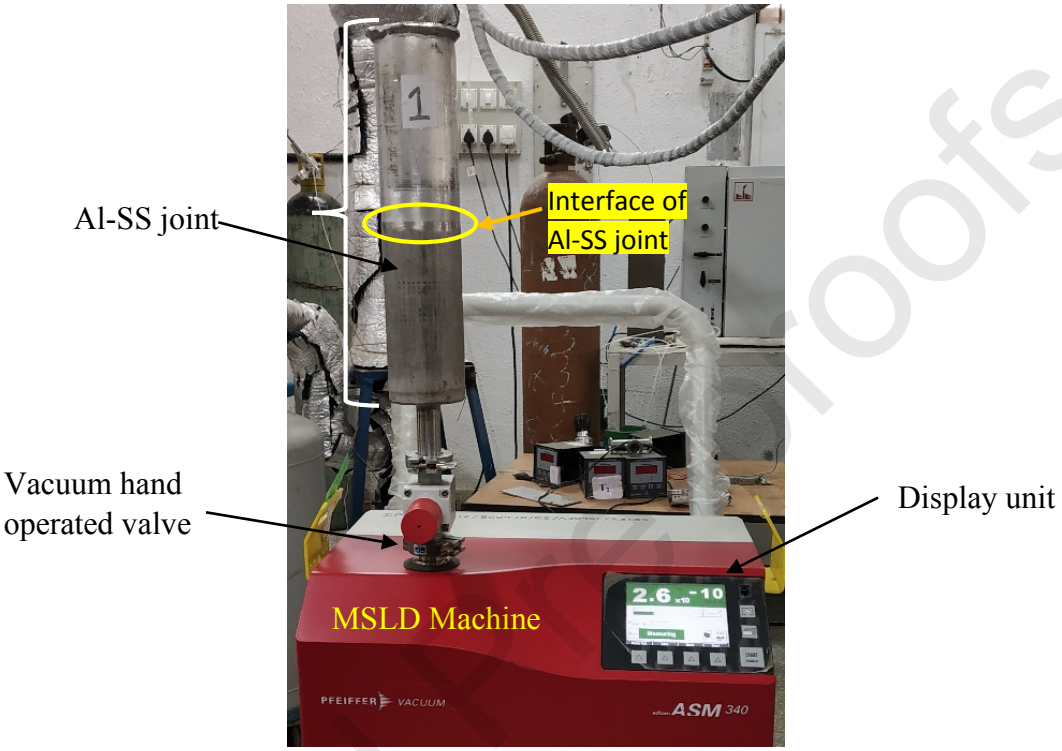

Figure 1. Experimental setup of vacuum test.

The tensile test was carried out as per specimen dimensions shown in Figure 2 from American society of mechanical engineers (ASME) section IX for welding qualification standard and regulation of pressure vessels. Tensile testing was performed using Universal Testing Machine, Make of Krutam Techno and Model of FSA/M-100. There were two samples extracted (from the full thickness of 5.4 mm) from each welded specimen using wire cut electro-discharge machining. All the specimens were subjected to tensile testing in order to select the specimen for further testing of microscopical characterizations. The fractured surfaces of tensile tests were analyzed using SEM. Microstructure studies were performed on the sample that is found with maximum tensile strength, using optical microscopy with the standard metallographic procedure of grinding and polishing followed by Keller's reagent etchant on the Al side. Additional polishing was carried out on the same sample for SEM, EDX, X-ray elemental mapping, and XRD analysis. This sample is further subjected to the microhardness

measurements with line mapping using NEXUS 4302 model of ESEWAY make machine, performed with load of 300 grams, at 100 µm intervals, from the center of the cross-section.

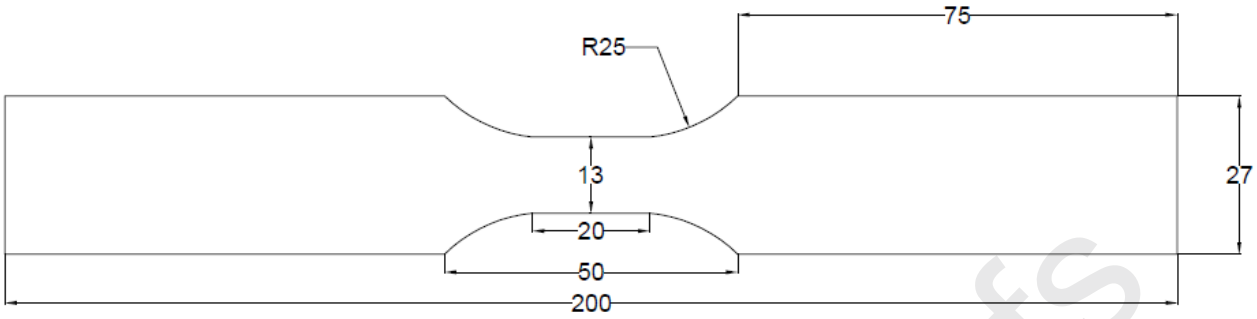

Figure 2. The dimension of a tensile specimen as per ASME sec IX (dimensions are in mm)

3. Results and discussion

3.1 Non-destructive tests

Visual inspection and liquid penetrant tests

Figure 3 shows the visual inspection of flash formation, wherein the first condition shows a small amount of flash formation from the outer surface and inner surface from the Al material. The selected parameters for the first condition were found less effective with small flash formation (see Figure 3). Therefore, an increase in friction time, friction force and burn off length was performed as shown in Table 3. With this condition 2, the flash formation from Al material was increased at the outer surface of a pipe compared to condition 1 as can be seen from Figure 3. However, the inner surface of the pipe was found with a smaller amount of flash formation. In order to create a large amount of flash formation, processing parameters were further increased in case of condition 3 as compared to conditions 1 and 2, as mentioned in Table 3. It can be observed from Figure 3 that a large amount of flash formation from outer and inner surfaces of pipe was obtained with condition 3, which in turn resulted in the higher length of Al sleeve formation on SS material. A large amount of flash formation can affect materials waste with more softening behavior of Al material. Therefore, condition 4 was selected to obtain flash formation in-between condition 3 and condition 2 with increased friction time, friction force, and decreased upset pressure, burn off length compared to condition 3. It can be seen from Figure 3 for condition 4 that the flash formation was reduced compared to condition 3 and increased compared to condition 1 and condition 2.

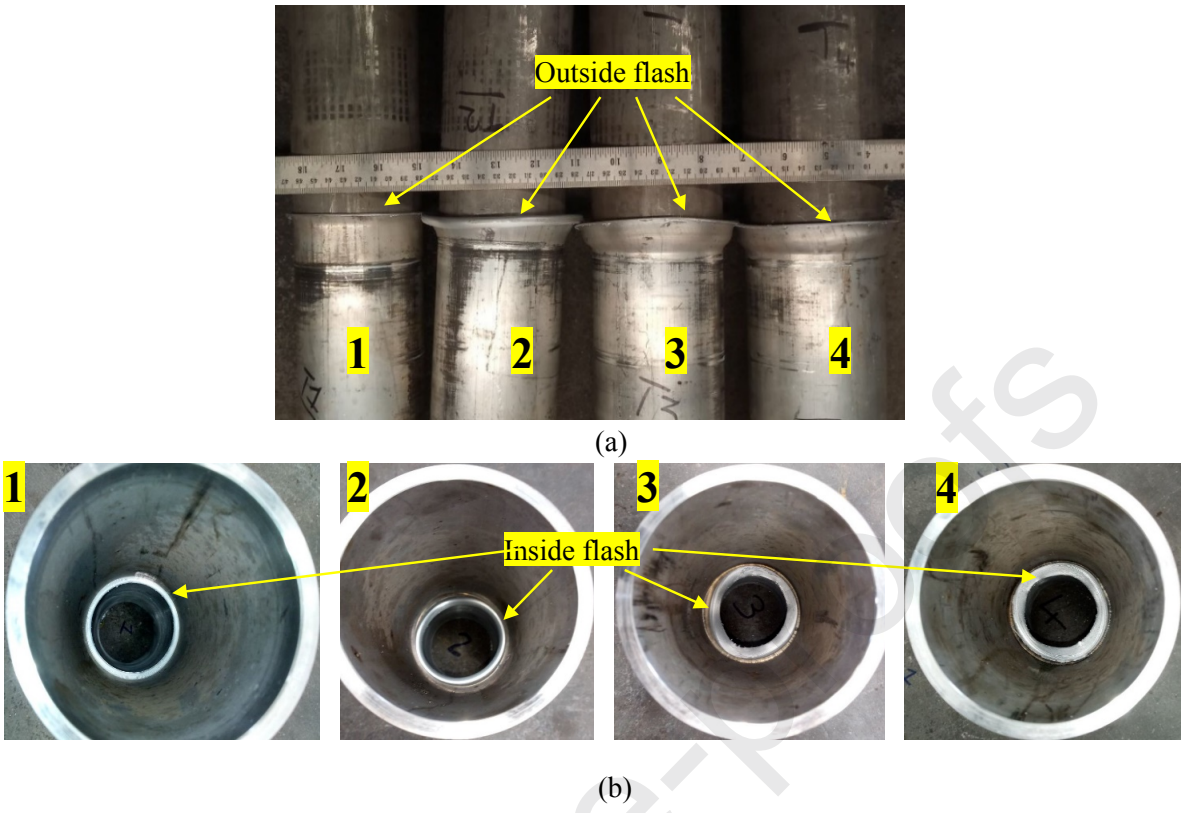

Figure 3. Flash formation inspection from (a) outer surface and (b) inner surface

The flash formation from the Al side was observed in all the conditions, whereas no macroscopic deformation of SS was observed. This is quite obvious and in line with the large softening behavior of Al compared to SS, which was also noticed in the previous literature of [10,22,36,37]. However, differences in flash formation have suggested parametric variations of experiments with different conditions. No other macroscopic discontinuities were observed in any of the samples. The welded joints were also inspected by dye penetrant test after removing flash and found defect free for all the processed conditions.

Vacuum leak detection, thermal shock, and pneumatic pressure tests

The vacuum leak detection test readings for as-welded samples at room temperature are shown in Table 4. All the samples were taken to the pressure in the range of 10^{-2} to 10^{-3} m bar background reading using the root rotary pump. Further, the pressure was reduced to the order of 10^{-10} m bar (i.e. ultra-high vacuum pressure) using MSLD system. The helium was sprayed on the outer surface of the joint area with 82 m bar pressure wherein vacuum pressure reading was noted on the other side. It can be seen from Table 4 that the leakage of helium was detected in the case of sample 2 based on leak rate observed after helium spray reading with a difference

of 1.3×10^{-4} m bar l/sec, whereas significant leak rate difference was not observed in other samples. In case of sample 2, the leak location was confirmed from the Al-SS joint interface using tacky tap application. The supporting welded joints were observed leak proof. The possibility of inconsistent bonding in circumferential weld with pipe configuration in friction welding may lead to this leak detection with unacceptable results, in case of sample 2. The upset pressure was low compared to all other processing parameters in case of sample 2 that may be the reason for inconsistent bonding in the circumferential weld that in turn resulted to leak detection.

Table 4. Vacuum leak detection test readings for as-welded samples in room temperature

Reading conditions / Samples Id	1	2	3	4
Background vacuum	9.4×10^{-3} m bar	2.1×10^{-2} m bar	1.4×10^{-2} m bar	1.2×10^{-2} m bar
Initial leak rate	2.7×10^{-10} m bar l/sec	4.3×10^{-8} m bar l/sec	5.1×10^{-10} m bar l/sec	2.8×10^{-10} m bar l/sec
Leak rate after helium spray	2.7×10^{-10} m bar l/sec	1.4×10^{-4} m bar l/sec	5.3×10^{-10} m bar l/sec	3.0×10^{-10} m bar l/sec
Remarks and interpretation	Acceptable without leak detection	Unacceptable with leak detection	Acceptable without leak detection	Acceptable without leak detection

In order to assess the compression and expansion behavior in cryogenic temperature, the thermal shocks were performed three times as mentioned in the materials and methods section. Figure 4 shows an image of samples after cryogenic thermal shocks. Table 5 presents the readings of helium leak detection test performed after cryogenic thermal shocks. The Sample 2 was unacceptable with leak detection difference of 3.3×10^{-4} m bar l/sec for the leak rate; besides, rest of the samples were observed leak proof. This proves that the reactive interface of dissimilar joints between Al-SS successfully experienced expansion and contraction under the thermal shocks and room temperature for samples 1, 3, and 4.

In the case of pneumatic test, it was observed that the welded pipes were capable to experience high pressure up to 25 bar (increased gradually) with working gas of helium. The sample 2 was also observed successful to sustain 25 bar pressure without any failure. It can be assumed that

the discontinuity on the interface between Al-SS of sample 2 was small enough influenced only in case of ultra-high vacuum condition and not in a high-pressure condition of 25 bar. It can also be predicted that the discontinuity was present somewhere on an interface with a tiny spot.

Figure 4. Samples after cryogenic thermal shocks

Table 5. Vacuum leak detection test readings of welded samples after cryogenic thermal shocks

Reading conditions / Samples Id	1	2	3	4
Background vacuum	9.4×10^{-3} m bar	7.0×10^{-2} m bar	1.0×10^{-2} m bar	1.0×10^{-2} m bar
Initial leak rate	3.9×10^{-10} m bar l/sec	4.5×10^{-8} m bar l/sec	1.9×10^{-9} m bar l/sec	2.0×10^{-10} m bar l/sec
Leak rate after helium spray	3.9×10^{-10} m bar l/sec	3.4×10^{-4} m bar l/sec	2.3×10^{-9} m bar l/sec	2.0×10^{-10} m bar l/sec
Remarks and interpretation	Acceptable without leak detection	Unacceptable with leak detection	Acceptable without leak detection	Acceptable without leak detection

3.2 Mechanical properties

Tensile properties

Figure 5 to Figure 8 show the results of the tensile testing of welded samples. Figure 5 shows the average yield strength, ultimate tensile strength (UTS) and % elongation from each condition subjected with two samples. Figure 6 presents stress-strain curve of tensile testing. The average UTS of 194.79 MPa was observed as a maximum in the case of sample 3, whereas the same was 136.46 MPa, 129.02 MPa, and 171.54 MPa in case of samples 1, 2 and 4 respectively. The noticeable difference between samples of 1, 2, and 3, 4 was a higher value of processing parameters. The upset pressure and burn off length were significantly (around 5 times) higher in the case of samples 3 and 4 compared to samples 1 and 2. Furthermore, the friction time and friction force were higher more than around 2 times in samples 3 and 4 as compared to samples 1 and 2. Higher friction time and force allow high heat input, which may be adequate to obtain viscoplastic effects in the base material. The higher upset pressure and burn off length also contribute to heat input conditions with enhancing timing with adequate pressure to promote interatomic diffusion as a joining mechanism. In case of AA6063 T6 and SS304L materials, the softening of Al material was obtained much earlier and hence resulted in large viscoplastic behavior. On the contrary, SS material was not observed with the large deformation due to higher melting temperature as compared to Al material. Therefore, increased upset pressure and burn off length have provided sufficient time to create a chemically active surface on the SS side with limited deformation and hence helped to obtain interatomic diffusion between largely deformed Al material and chemically active SS surface that in turn resulted with higher tensile strength. In sample 4, the tensile strength was reduced as compared to sample 3, wherein the upset pressure was reduced and friction time, friction force and burn off length were increased. Despite of increased friction time, friction force and burn off length, the tensile strength was reduced because the upset pressure was reduced that may have affected interatomic diffusion with inadequate pressure. The maximum obtained UTS of 194.79 MPa was 72% of the AA6063-T6 material, which can be considered as an acceptable range of dissimilar pipe welded joints of AA6063-T6 and SS304L combination. So far, in pipe friction welding of Al-SS combination, the obtained joint efficiency of 72% in the present investigation was highest as compared to published literature of [10,27,34]. The presence of IMCs at the interface may be the reason for less joint efficiency as they were known for the deterioration of mechanical properties. However, the synergic effects of mechanical bonding and metallurgical bonding induced by the Al/Fe IMC layer also contributes to the high UTS [34, 36]. Similar to the trend observed in ultimate tensile strength, the yield strength of

155.76 MPa was highest in sample 3 compared to other samples of 1, 2, and 4. This shows sound interatomic diffusion bonding with the possibilities of a thin IMCs layer. The results and discussion on the formation of IMCs are presented in the subsequent section. Moreover, the elongation of welded joints was observed in a range of 7 to 10 % as can be seen from Figure 5, which was lower than the base material of AA6063-T6 and SS304L. Usually, in the case of Al-SS welding, the elongation of a welded specimen found low due to the formation of IMCs [15,38]. The necking in the tensile specimen was absent as can be seen from Figure 7 that represents fractured tensile specimens of sample 3, which supports low elongation observed. The results obtained from tensile testing can be correlated from stress-strain curve as shown in Figure 6. The proportional limit and necking regions were limited that generally observed in case of brittle material. Therefore, low elongation and yield strength values were observed. One tensile specimen of leak detected sample 2 was observed with low UTS such as 72 MPa. It can be seen from Figure 7 that the samples were fractured from the joint interface between Al-SS materials. The SEM images of fractured surfaces can be seen from Figure 8, wherein flat surface was observed on the SS with large scale image (refer Figure 8 (a)). However, dimple like structure was observed in a magnified scale, as can be seen from Figure 8 (b). The flat surface at the macro level was observed because the fracture occurred from the interface between Al-SS. Besides, the dimples on the SS side were observed due to grains fracture effect of Al material that was bonded to SS. In case of Al fractured surface, a large number of dimples were observed as can be seen from Figure 8 (c) and (d). This shows that the fractured occurred from a bonded region of Al-SS interface with dimples formation of Al material. A similar fracture was found in the literature of [14,22,26,35]. Figure 8 (c) and (d) show that the layer type structures were noticed at different locations (at micro level), which can be predicted as IMCs based on flat layer characteristics. These IMCs in turn promoted localized brittle fractures at specific locations with their known hard and brittle characteristics. The low elongation observed in Figure 5 can be correlated from these IMCs that promoted failure before necking occurs (refer Figure 6). Hence, it can be said that the fracture was a mixture of brittle and ductile modes, dominated by a brittle fracture with local IMCs layers and the flat surfaces on the SS side.

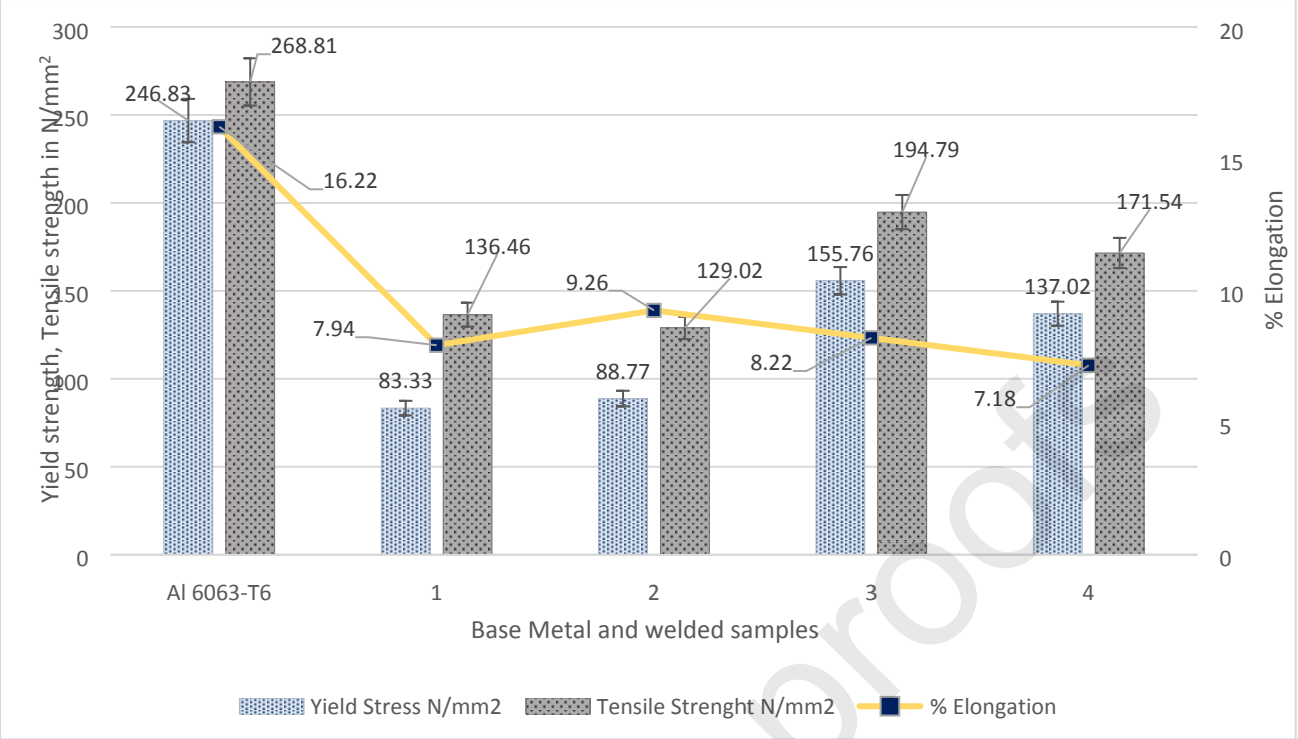

Figure 5. Tensile testing results

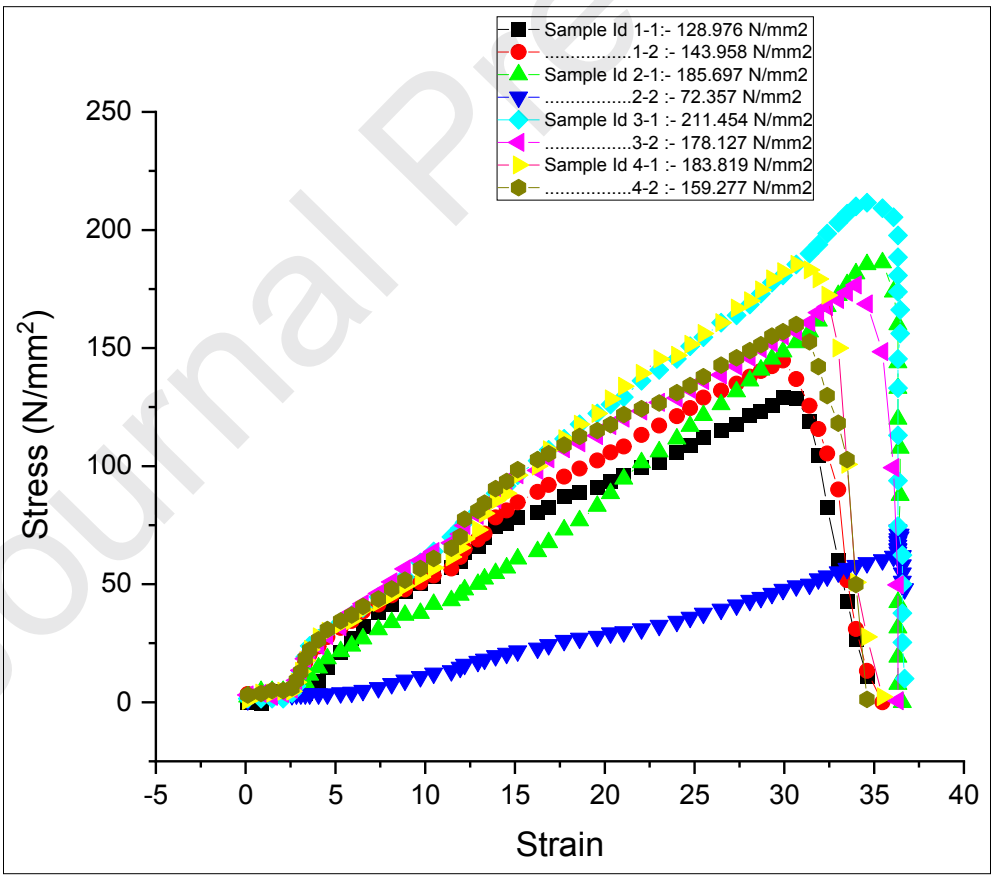

Figure 6. Stress-strain curve of tensile testing.

Figure 7. Fractured tensile specimens of sample 3

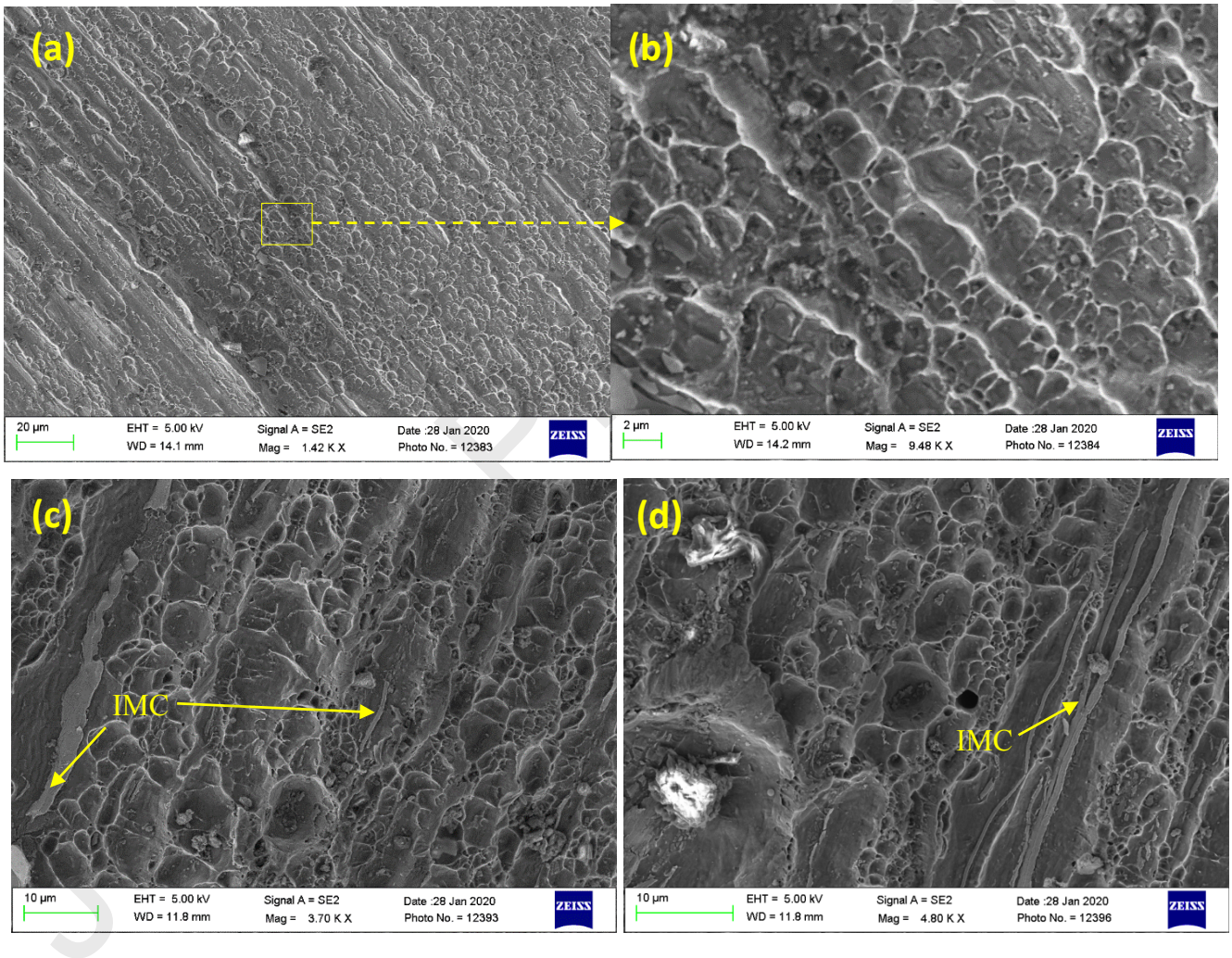

Figure 8. SEM fracture surface images of sample 3 (a)-(b) SS side and (c)-(d) Al side

Hardness measurements

Figure 9 shows hardness measurements across the cross-section of dissimilar Al-SS welded sample 3. The hardness of the joint line was nearly equal to the AA6063-T6 material. No major variations either in AA6063-T6 or SS304L in hardness values near to the joint line were

observed. The deformation and recrystallization cannot be avoided at the Al side due to mechanical load under the action of frictional heat that is presented in the subsequent section. Despite the fact of change in microstructures, the hardness of Al material near to joint line was not much affected. SS304L side hardness peaks were observed three times higher than Al material. A similar trend of hardness variations was observed in the literature of [28,33], wherein the narrow width of a deformed zone was mentioned as the cause of minor change in hardness near a joint line towards the Al side.

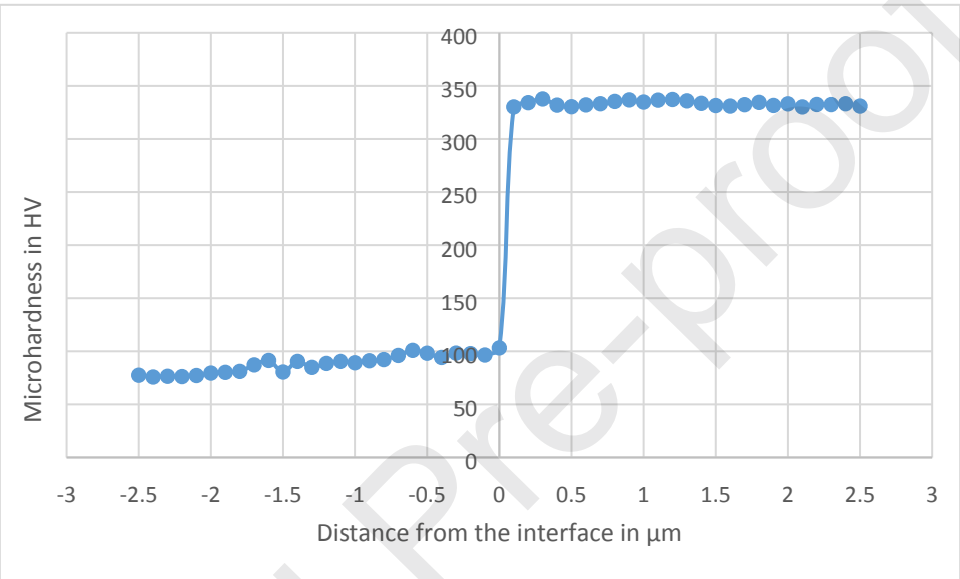

Figure 9. Hardness distribution across a cross-section of sample 3 joint

3.2 Microstructure and characterization

Optical microscopy

Figure 10 shows the macrograph and microstructure features of the Al-SS friction welded joint conditioned sample 3. Figure 10 (M) shows that the distinct interface between Al-SS along with grain change effects towards Al side. The microstructure changes on the Al side near to the weld interface were divided into different categories of the recrystallized zone (RZ), plastic deformation zone (PDZ), solid solution zone, partially recrystallized zone (PRZ), and partially secondary recrystallized zone (PSRZ) as shown in Figure 10 (c)-(f). Figure 10 (a) and (b) show the microstructure of SS304L and AA6063-T6 respectively. Figure 10 (c) and (e) show black color interface between Al-SS, which may be of oxide layer along with reaction layer of Al-Fe interactions. The microstructure of SS304L shows austenitic type structure with twin grain boundaries, whereas the microstructure of AA6063-T6 shows elongated grains with precipitates distributed in direction of rolling. After the friction welding, the AA6063-T6 leads

to the viscoplastic effect and resulted as sleeve formation on top of SS material. This in turn influenced microstructure near to the weld interface. At the interface towards the edge of pipe (i.e. location C mentioned in (M) of Figure 10), the grains were elongated in the direction of flash movement and identified as very fine compared to base material AA6063-T6. These grains were formed due to recrystallization after the viscoplastic effect as the material of AA6063-T6 near the Al-SS interface experienced recrystallization temperature. Recrystallized grains were also presented throughout the cross-section near to the interface. However, in the middle of the cross-section, near to the interface, the grains experienced recrystallized temperature and consolidated within the region without materials movement (i.e. without elongation). The material at the edge cannot be restricted for consolidation within the zone as the outer surface was open. Furthermore, the solid solution zone was identified as can be seen from Figure 10 (e) within this recrystallized zone, very close to the interface between Al-SS. In this zone, the temperature was highest being the closest zone of the Al-SS interface, wherein the cooling rate was also high that in turn lead to insufficient time for the effect of secondary phase precipitation and results into solid solution zone. Similar zones were observed in the literature [29]. Besides the recrystallized zone, the plastic deformation zone was found as shown in Figure 10 (d), wherein the grains were affected by mechanical deformation and thermal effects without recrystallization. This zone was away from the interface between Al-SS and due to that the recrystallization temperature was not reached and hence only influenced by mechanical deformation and conducted heat. However, within this zone, some region was found with partial secondary recrystallization as shown in Figure 10 (f) influenced by high heat conduction.

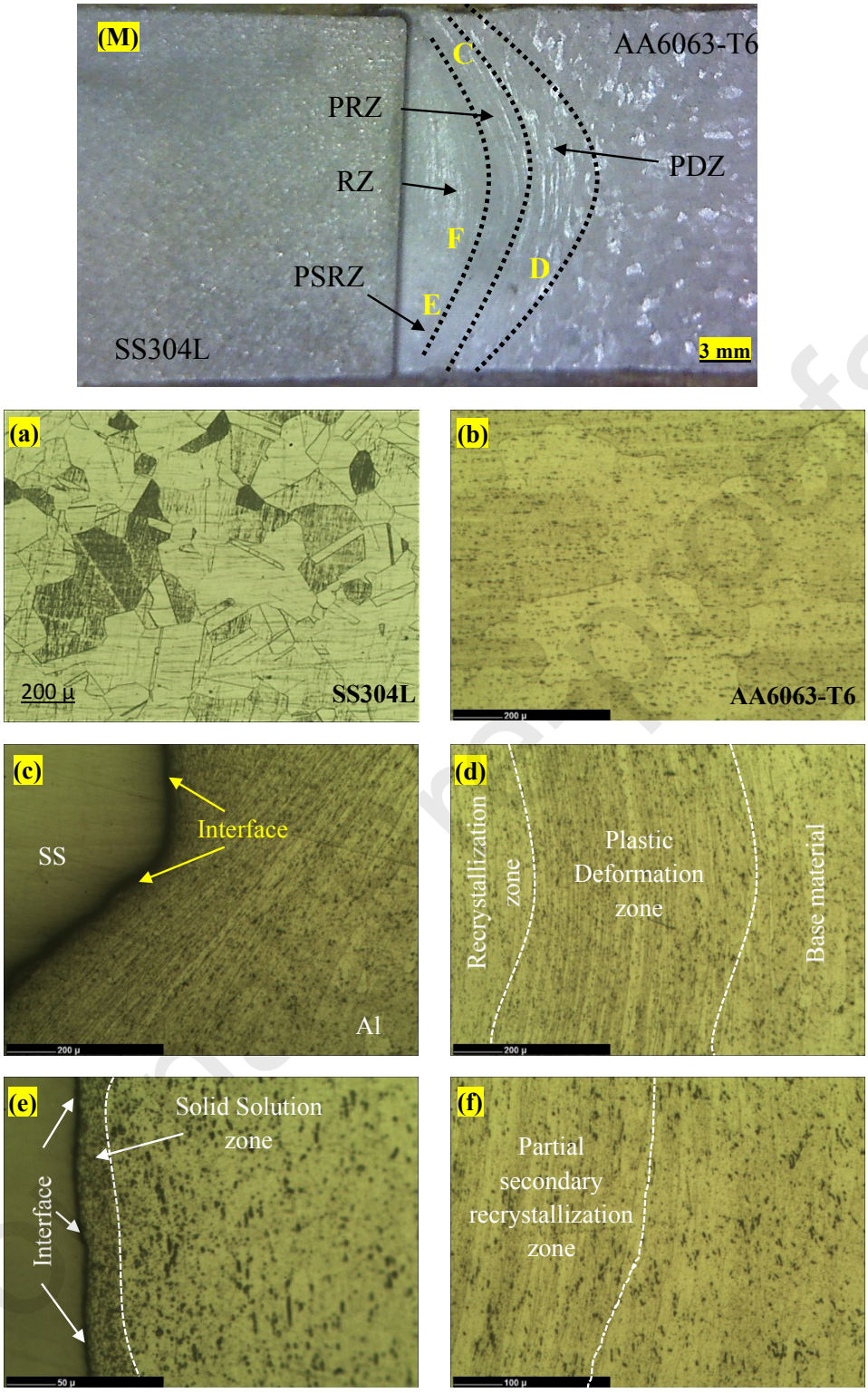

Figure 10. (M) Macrostructure: recrystallized zone (RZ), plastic deformation zone (PDZ), solid solution zone, partially recrystallized zone (PRZ), and partially secondary recrystallized zone (PSRZ); and (a)-(f) Microstructures of Sample 3: (a) SS304L base material , (b) AA6063-T6 base material, (c) SS-Al interface at edge, (d) different deformation zones at Al side, (e) solid solution and interface (f) partial secondary recrystallized zone

Electron microscopy and X-ray diffractions

The reaction layer between Al-SS was investigated by X-ray elemental mapping and EDX along with its measurements by SEM. Thin reactive layer in between Al-SS materials can be observed in Figure 11 of SEM image and X-ray elemental mapping. The reaction between Al-SS material leads to the formation of IMCs under the effect of solid-state interdiffusion on chemically active surfaces. Table 6 shows the thickness of a reaction layer at different spots. The reaction layer was found as continuous with varying thickness in between 1.1 µm to 2.0 µm. The average thickness of a reaction layer was found at 1.4 µm (with five different measurements as presented in Table 6). No major variation in reaction layer thickness was observed throughout the diameter of the Al-SS interfaced to the pipe configuration consisting of a radial area to form a reaction within the given heat input. The reaction layer growth was governed by heat input conditions and time of reaction [30, 31]. In friction welding, the maximum temperature is assumed below 600°C considering operating process principle in solid-state with 80% of melting temperature of base material, hence the solid-state interdiffusion was the cause of this reaction layer.

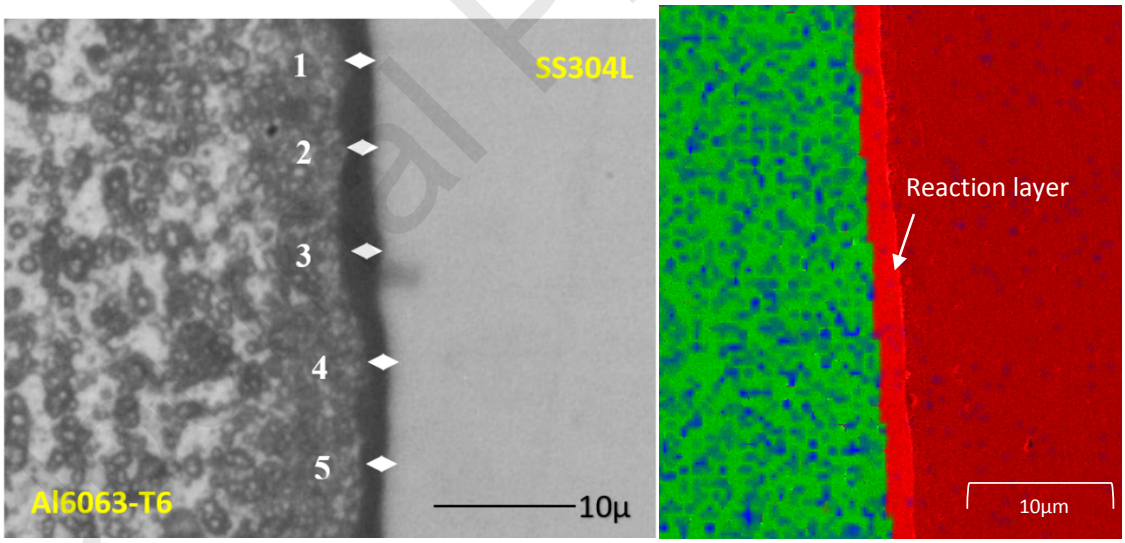

(a) (b)

Figure 11. Al-SS interface (a) SEM image and (b) X-ray elemental mapping

Table 6. Measurements of reaction layer between the Al-SS joint corresponding to Figure 11.

Location	Measurement (μm)
1	1.3
2	1.3
3	2.0
4	1.1
5	1.2
Average	1.4

The reaction layer was confirmed by line scanning using EDX as shown in Figure 12, wherein the focus of scanning was kept on Al and Fe as shown by EDX signals for respective elements. At the interface region, it can be seen that the elements were interacted crossing each other with line scanning. This supports the participation of Al and Fe in formation of reaction layer, as mentioned above with Figure 11. Figure 13 shows X-Ray Diffraction (XRD) results that were performed to identify the IMC's presence with a specific phase identification. The IMC of Fe_3Al was identified along with Al and Fe elements from diffraction peaks. The reaction of Fe-Al elements under the solid-state temperature of AA6063-T6 (i.e. below 600°C) led the formation of nonstoichiometric compound Fe_3Al resulted from solid-state interdiffusion with the participation of 30 % Fe and 20 % Al based on the binary phase diagram of Al-SS [32].

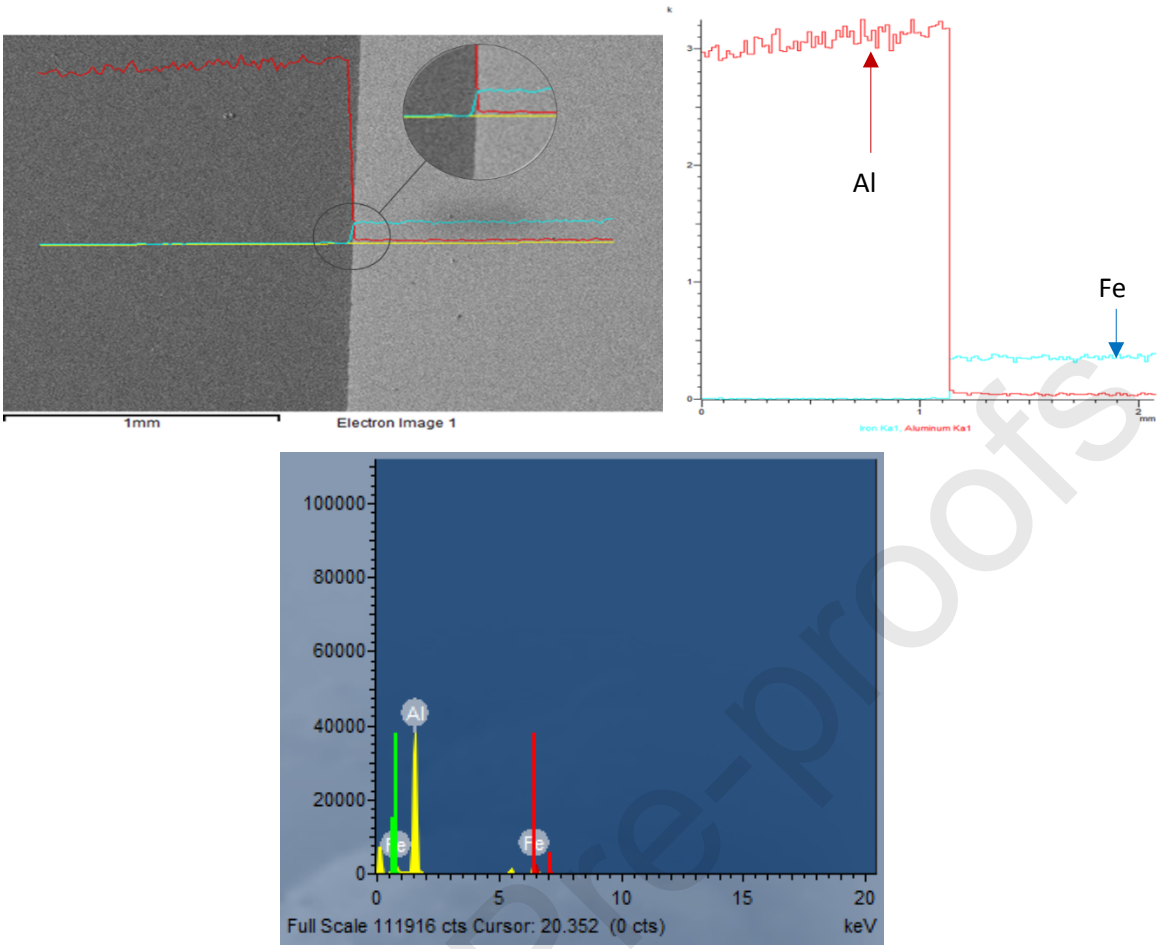

Figure 12. EDX line scanning results of the Al-SS interface of sample 3.

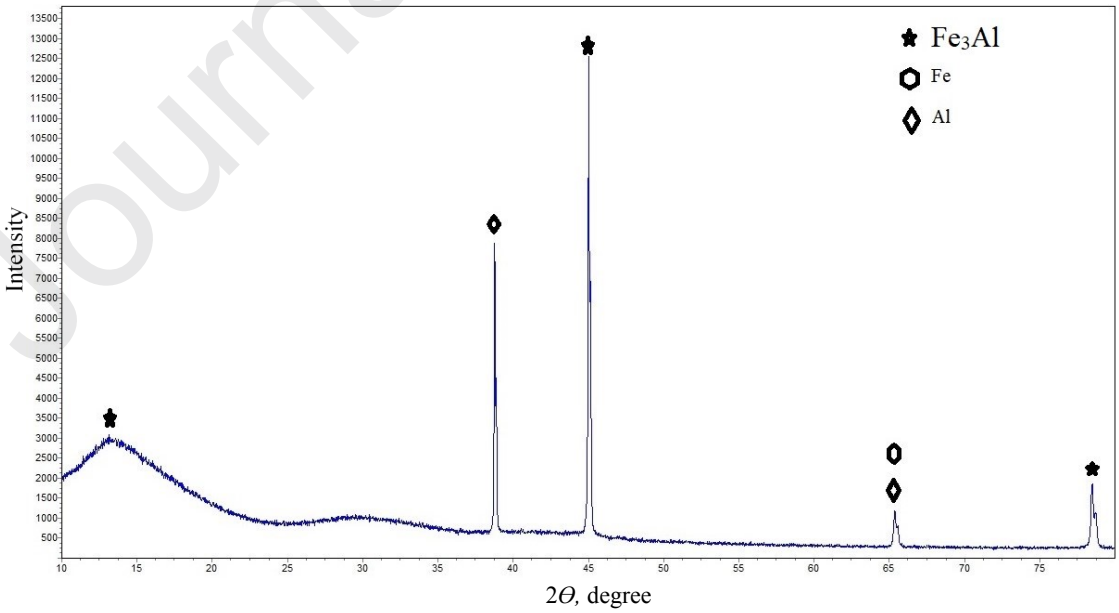

Figure 13. XRD for phase identification in case of sample 3

Conclusions

The present investigation explored manufacturing and quality assessments of dissimilar Al-SS friction welding for pipe joint configuration with an outer diameter of 88.90 mm and 5.4 mm thickness (i.e. ratio of pipe thickness to diameter is 0.060). Specific conclusive statements on this investigation can be drawn as follows.

(1) Pipe configuration with a higher outer diameter and wall pipe thickness can be successfully welded by friction welding for dissimilar Al-SS joints.

(2) Suitability of Al-SS bimetallic welded pipes evaluated for ultra-high vacuum applications and cryogenic working environments. The Al-SS joint of condition 3 (performed by the rotational speed of 350 rpm, upset time of 5 seconds, friction time of 15 seconds, friction force of 8.2 Tones, upset pressure of 16.4 Tones, burn off length of 25.1 mm) operated with ultra-high vacuum and high pressurized conditions without leak detection.

(3) Maximum tensile strength of 194.79 MPa was obtained with pipe configuration for condition 3. The joint efficiency of 72 % of AA6063-T6 was noticed as highest among published literature on Al-SS pipe friction welds hitherto. The tensile fracture was identified as a mixture of brittle and ductile modes, dominated by a brittle fracture with local intermetallic compound layers and a flat surface on the SS side.

(4) Microstructure changes were observed largely towards the Al side close to the Al-SS interface. Al material near the Al-SS interface experienced full and partial recrystallization with the presence of solid solution zone and mechanically deformed zones progressively towards a base material direction.

(5) The reaction layer between Al-SS joints under condition 3 was found as continuous with varying thickness in between 1.1 μm to 2.0 μm (i.e. average thickness of 1.4 μm). The intermetallic compound of the Fe_3Al phase was identified as a result of the reaction between Al-Fe elements from the reaction layer.

Acknowledgments

The funding from the Board of Research in Nuclear Sciences-India (Project No: 39/14/02/2018-BRNS/39002), experimentation help from Vulcan Industrial Engineering and execution of helium leak detection test from Institute for Plasma Research-Gandhinagar (support from Mr. A K Sahu) are sincerely acknowledged.

References

[1] S. Shankar, P. Vilaça, P. Dash, S. Chattopadhyaya, S. Hloch, Joint strength evaluation of friction stir welded Al-Cu dissimilar alloys, Meas. J. Int. Meas. Confed. 146 (2019) 892–902. https://doi.org/10.1016/j.measurement.2019.07.019.

[2] N.P. Patel, P. Parlikar, R. Singh Dhari, K. Mehta, M. Pandya, Numerical modelling on cooling assisted friction stir welding of dissimilar Al-Cu joint, J. Manuf. Process. 47 (2019) 98–109. https://doi.org/10.1016/j.jmapro.2019.09.020.

[3] M. Paidar, S. Ghavamian, O.O. Ojo, A. Khorram, A. Shahbaz, Modified friction stir clinching of dissimilar AA2024-T3 to AA7075-T6: Effect of tool rotational speed and penetration depth, J. Manuf. Process. 47 (2019) 157–171. https://doi.org/10.1016/j.jmapro.2019.09.028.

[4] K.P. Mehta, R. Patel, H. Vyas, S. Memon, P. Vilaça, Repairing of exit-hole in dissimilar Al-Mg friction stir welding: Process and microstructural pattern, Manuf. Lett. 23 (2020) 67–70. https://doi.org/10.1016/j.mfglet.2020.01.002.

[5] K.P. Mehta, P. Carlone, A. Astarita, F. Scherillo, F. Rubino, P. Vora, Conventional and cooling assisted friction stir welding of AA6061 and AZ31B alloys, Mater. Sci. Eng. A. 759 (2019) 252–261. https://doi.org/10.1016/j.msea.2019.04.120.

[6] Q. Li, Z. Ma, S. Ji, Q. Song, P. Gong, R. Li, Effective joining of Mg/Ti dissimilar alloys by friction stir lap welding, J Mater Process Tech 278 (2020) 116-483. https://doi.org/10.1016/j.jmatprotec.2019.116483

[7] K.P. Mehta, V.J. Badheka, Hybrid approaches of assisted heating and cooling for friction stir welding of copper to aluminum joints, J. Mater. Process. Technol. 239 (2017) 336–345. https://doi.org/10.1016/j.jmatprotec.2016.08.037.

[8] K.P. Mehta, V.J. Badheka, A review on dissimilar friction stir welding of copper to aluminum: Process, properties, and variants, Mater. Manuf. Process. 31 (2016) 233–254. https://doi.org/10.1080/10426914.2015.1025971.

[9] K.P. Mehta, V.J. Badheka, Effects of tilt angle on the properties of dissimilar friction stir welding copper to aluminum, Mater. Manuf. Process. 31 (2016) 255–263. https://doi.org/10.1080/10426914.2014.994754.

[10] H. Vyas, K.P. Mehta, V. Badheka, B. Doshi, Pipe - to - pipe friction welding of dissimilar Al - SS joints for cryogenic applications, J. Brazilian Soc. Mech. Sci. Eng. 1 (2020). https://doi.org/10.1007/s40430-020-2181-1.

[11] L.H. Shah, M. Ishak, Review of research progress on aluminum-steel dissimilar welding, Mater. Manuf. Process. 29 (2014) 928–933.

https://doi.org/10.1080/10426914.2014.880461.

[12] K.P. Mehta, A review on friction-based joining of dissimilar aluminum-steel joints, J. Mater. Res. 34 (2019) 78–96. https://doi.org/10.1557/jmr.2018.332.[13] M. Habibi, R. Hashemi, M. Fallah Tafti, A. Assempour, Experimental investigation of mechanical properties, formability and forming limit diagrams for tailor-welded blanks produced by friction stir welding, J. Manuf. Process. 31 (2018) 310–323. https://doi.org/10.1016/j.jmapro.2017.11.009.

[14] H. Dong, J. Yang, Y. Li, Y. Xia, X. Hao, P. Li, D. Sun, J. Hu, W. Zhou, M. Lei, Evolution of interface and tensile properties in 5052 aluminum alloy/304 stainless steel rotary friction welded joint after post-weld heat treatment, J. Manuf. Process. 51 (2020) 142–150. https://doi.org/10.1016/j.jmapro.2020.01.038.

[15] Y. Liu, H. Zhao, Y. Peng, X. Ma, Microstructure characterization and mechanical properties of the continuous-drive axial friction welded aluminum/stainless steel joint, Int. J. Adv. Manuf. Technol. 104 (2019) 4399–4408. https://doi.org/10.1007/s00170-019-04245-5.[16] K.P. MEHTA, V.J. BADHEKA, Influence of tool pin design on properties of dissimilar copper to aluminum friction stir welding, Trans. Nonferrous Met. Soc. China (English Ed. 27 (2017) 36–54. https://doi.org/10.1016/S1003-6326(17)60005-0.

[17] R. Paventhan, P.R. Lakshminarayanan, V. Balasubramanian, Prediction and optimization of friction welding parameters for joining aluminium alloy and stainless steel, Trans. Nonferrous Met. Soc. China (English Ed. 21 (2011) 1480–1485. https://doi.org/10.1016/S1003-6326(11)60884-4.

[18] E.P. Alves, F.P. Neto, C.Y. An, Welding of AA1050 aluminum with AISI 304 stainless steel by rotary friction welding process, J. Aerosp. Technol. Manag. 2 (2010) 301–306. https://doi.org/10.5028/jatm.2010.02037110.

[19] S. Fukumoto, H. Tsubakino, K. Okita, M. Aritoshi, T. Tomita, Microstructure of friction weld interface of 1050 aluminium to austenitic stainless steel, Mater. Sci. Technol. 14 (1998) 333–338. https://doi.org/10.1179/mst.1998.14.4.333.

[20] W.B. Lee, Y.M. Yeon, D.U. Kim, S.B. Jung, P. Jung, Effect of friction welding parameters on mechanical and metallurgical properties of aluminium alloy 5052-A36 steel joint, (n.d.) 449–910. https://doi.org/10.1179/026708303225001876.

[21] T. Yokoyama, K. Ogawa, Impact tensile properties of 6061 aluminium alloy to SUS 304 stainless steel friction-welded butt joints, Weld. Int. 17 (2003) 514–523. https://doi.org/10.1533/wint.2003.3118.

[22] M. Kimura, K. Suzuki, M. Kusaka, K. Kaizu, Effect of friction welding condition on joining phenomena and mechanical properties of friction welded joint between 6063 aluminium alloy and AISI 304 stainless steel, J. Manuf. Process. 26 (2017) 178–187. https://doi.org/10.1016/j.jmapro.2017.02.008.

[23] S. Fukumoto, H. Tsubakino, K. Okita, M. Aritoshi, T. Tomita, Static joint strength of friction welded joint between aluminium alloys and stainless steel, Weld. Int. 14 (2000) 89–93. https://doi.org/10.1080/09507110009549145.

[24] M. Yilmaz, M. Çöl, M. Acet, Interface properties of aluminum/steel friction-welded components, Mater. Charact. 49 (2002) 421–429. https://doi.org/10.1016/S1044-5803(03)00051-2.

[25] S.D. Meshram, G. Madhusudhan Reddy, Friction welding of AA6061 to AISI 4340 using silver interlayer, Def. Technol. 11 (2015) 292–298. https://doi.org/10.1016/j.dt.2015.05.007.

[26] H. Wang, G. Qin, P. Geng, X. Ma, Interfacial microstructures and mechanical properties of friction welded Al / steel dissimilar joints, J. Manuf. Process. 49 (2020) 18–25. https://doi.org/10.1016/j.jmapro.2019.11.009.

[27] M. Kimura, M. Kusaka, K. Kaizu, K. Nakata, K. Nagatsuka, Friction welding technique and joint properties of thin-walled pipe friction-welded joint between type 6063 aluminum alloy and AISI 304 austenitic stainless steel, Int. J. Adv. Manuf. Technol. 82 (2016) 489–499. https://doi.org/10.1007/s00170-015-7384-8.

[28] Y. Liu, H. Zhao, Y. Peng, X. Ma, Mechanical properties of the inertia friction welded aluminum/stainless steel joint, Weld. World. 63 (2019) 1601–1611. https://doi.org/10.1007/s40194-019-00793-2.

[29] L. Wan, Y. Huang, Friction welding of AA6061 to AISI 316L steel: characteristic analysis and novel design equipment, Int. J. Adv. Manuf. Technol. 95 (2018) 4117–4128. https://doi.org/10.1007/s00170-017-1505-5.

[30] H. Springer, A. Kostka, E.J. Payton, D. Raabe, A. Kaysser-Pyzalla, G. Eggeler, On the formation and growth of intermetallic phases during interdiffusion between low-carbon steel and aluminum alloys, Acta Mater. 59 (2011) 1586–1600. https://doi.org/10.1016/j.actamat.2010.11.023.

[31] S. Fukumoto, H. Tsubakino, K. Okita, M. Aritoshi, T. Tomita, Friction welding process of 5052 aluminium alloy to 304 stainless steel, Mater. Sci. Technol. 15 (2013) 1080–1086. https://doi.org/10.1179/026708399101506805.

[32] F. Haidara, M.C. Record, B. Duployer, D. Mangelinck, Phase formation in Al-Fe thin

film systems, Intermetallics. 23 (2012) 143–147. https://doi.org/10.1016/j.intermet.2011.11.017.

[33] F. Filho, S. Monteiro, Welding Joints in High Entropy Alloys: A Short-Review on Recent Trends, J Mater Sci & Technol 45, 2020, 59-69. https://doi.org/10.3390/ma13061411

[34] Y. Huang, T. Huang, L. Wan, X. Meng, L. Zhou, Material flow and mechanical properties of aluminum-to-steel self-riveting friction stir lap joints. J. Mater. Process Tech. 263, (2019) 129-137. https://doi.org/10.1016/j.jmatprotec.2018.08.011

[35] P. Li, H. Donga, Y. Xiaa, X. Haoa, S. Wanga, L. Pana, J. Zhoub, Inhomogeneous interface structure and mechanical properties of rotary friction welded TC4 titanium alloy/316L stainless steel joints. J. Manuf. Process. 33, (2018) 54-63. https://doi.org/10.1016/j.jmapro.2018.05.001

[36] Y. Huang, L. Wan, X. Si, T. Huang, X. Meng, and Y. Xie, Achieving High-Quality Al/Steel Joint with Ultrastrong Interface. Metall and Mat Trans A 50, 295–299 (2019). https://doi.org/10.1007/s11661-018-5006-4

[37] J. Mohammadi, Y. Behnamian, A. Mostafaei, A. P. Gerlich, Tool geometry, rotation and travel speeds effects on the properties of dissimilar magnesium/aluminum friction stir welded lap joints, Materials & Design 75 (2015): 95-112. https://doi.org/10.1016/j.matdes.2015.03.017

[38] J. Mohammadi, A. Mostafaei, H. Izadi, T. Saeid, A. H. Kokabi, A. P. Gerlich, Friction stir welding joint of dissimilar materials between AZ31B magnesium and 6061 aluminum alloys: Microstructure studies and mechanical characterizations. Materials Characterization 101 (2015): 189-207. https://doi.org/10.1016/j.matchar.2015.01.008

The authorship credit is identified as under for associated authors.

Hardik D. Vyas performed and coordinated all the experiments, prepared a first draft of the manuscript, working as senior research fellow and doctoral student.

Kush P. Mehta performed draft modifications and revisions, worked on conceptualization, results interpretation and analysis, main supervisor of doctoral candidate supervision, principle investigator for funded project, responsible for funding acquisition and execution.

Vishvesh Badheka collaborated for experimental facilities used in this investigation, co-supervisor of doctoral candidate supervision, co-principle investigator of funded project and project execution.

Bharat Doshi is principle collaborator from funding agency with overall supervision and project execution.

- Processing and evaluation of Al-SS bimetallic friction welding for pipe configuration.
- The joint efficiency 72 % of Al base material is obtained.
- The reaction layer between Al-SS is measured between 1.1 μm to 2.0 μm.